Regular Article

Cold-induced Conversion of Connective Tissue Skeleton in Brown Adipose Tissues

Masako Yudasaka[1,2], Yuko Okamatsu-Ogura[3], Takeshi Tanaka[1], Kumiko Saeki[4,5] and Hiromichi Kataura[1]

[1]Nanomaterials Research Institute, National Institute of Advanced Industrial Science and Technology, Tsukuba, Ibaraki 305–8565, Japan, [2]Graduate School of Science and Technology, Meijo University, Nagoya 468–8502, Japan, [3]Laboratory of Biochemistry, Faculty of Veterinary Medicine, Hokkaido University, Sapporo 060–0818, Japan, [4]Department of Laboratory Molecular Genetics of Hematology, Graduate School of Medical and Dental Sciences, Tokyo Medical and Dental University, Tokyo 113–8510, Japan and [5]Department of Regenerative Medicine, Research Institute, National Center for Global Health and Medicine, Tokyo 162–8655, Japan

Thermogenesis *via* fatty acid-induced uncoupled mitochondrial respiration is the primary function of brown adipose tissue (BAT). In response to changes in ambient temperatures, the weight and specific gravity of BAT change, depending on the quantity of lipid droplets stored in brown adipocytes (BA). Such conditions should result in the reconstruction of connective tissue skeletons, especially of collagen fiber networks, although the mechanisms have not been clarified. This study showed that, within 4 hr of exposing mice to a cold environment, collagen fibers in the extracellular matrix (ECM) of BAT became discontinuous, twisted, emancipated, and curtailed. Surprisingly, the structure of collagen fibers returned to normal after the mice were kept at room temperature for 19 hr, indicating that the alterations in collagen fiber structures are physiological processes association with adaptation to cold environments. These dynamic changes in connective tissue skeletons were not observed in white adipose tissues, suggesting that they are unique to BAT. Interestingly, the vascular permeability of BAT was also augmented by exposure to cold. Collectively, these findings indicate that dynamic changes in ECM collagen fibers provide high flexibility to BAT, enabling the adjustment of tissue structures and the regulation of vascular permeability, resulting in adaptation to changes in ambient temperatures.

Key words: brown adipose tissue, cold stimuli, collagen fibers, extravasation, near infrared fluorescence microscopy

I. Introduction

Collagens are the major components of extracellular matrices (ECMs), which assemble to form fibers and sheets. More than 30 collagen subtypes have been identified to date. Structurally, collagen molecules form triple helices, enhancing the mechanical strength of connective tissues. Collagens also maintain the physiological integrity

Correspondence to: Masako Yudasaka, National Institute of Advanced Industrial Science and Technology (AIST), Central 5–2, 1–1–1 Higashi, Tsukuba 305–8565, Japan.
E-mail: m-yudasaka@aist.go.jp, yudasaka.masako@gmail.com

and homeostasis of tissues.

Five major types of collagen molecules have been studied to date. About 90% of collagen molecules in the body are type I, and their fibers are mainly found in skin, tendons, and non-mineral parts of bones. Cartilage is formed by type II collagens, together with proteoglycans. Type IV collagens do not form fibers and are found in the basement membranes. Type V collagens are found in hair and nails. Type III collagens (Col. III) form network-like fibers, which are called reticular fibers to differentiate them from other bundle-shaped collagen fibers. Col. III fibers, which are finer than types I and II collagen fibers and can be detected by silver impregnation staining [17, 24], are

mainly found in reticular organs, such as bone marrow, liver, spleen, and lymphoid tissues [3, 24].

In addition to reticular organs, Col. III fibers are present in adipose tissues [22]. Less is known, however, about whether Col. III is present in brown adipose tissues (BATs), although silver impregnation staining showed that ECM of BAT contains Col. III fibers [27]. BAT size is significantly reduced under fasting conditions due to the metabolism of lipid droplets, the major constituents of the cytoplasm of brown adipocytes (BA) [27]. Interestingly, the expression of matrix metalloproteinase-3 is upregulated in fasted mice, and collagen fibers in BAT are disordered and degenerated. As a result, the permeability of capillaries and arterioles is enhanced, as visualized by the extravasation of nanomaterials of single-walled carbon nanotubes (CNTs) [27]. Our previous studies used CNTs [10, 11] because they emit near infrared (NIR) fluorescence (wavelength > 1000 nm) [19]. Light of this wavelength is suitable for biological imaging because its wavelength is outside the bio-autofluorescence wavelength region and is less absorbed and less scattered by biological materials [23]. Importantly, the collagen fibers that had degenerated undergo prompt reconstruction within 1 day and the structures of BAT return to normal, suggesting that changes in collagen fibers in BAT are physiological responses [27]. The highly flexible structure of collagen fibers is beneficial for BATs, enabling them to adapt to an acute shrinkage in BAs without loss of physiological functions. If the dynamic changes in collagen fiber structures in BAT are adaptations to life-threatening situations, such as fasting, similar remodeling would likely occur in other critical situations.

The present study shows that comparable changes in the structure of collagen fiber occur in BATs of cold-stimulated mice. Although cold stimulation has been reported to alter BAT activities [1, 2, 6, 14], by, for example, enhancing triglyceride consumption [2], the overall molecular mechanisms remain unclear. Studies have shown that cold stimulation in associated with the browning of white adipose tissues (WAT), generating beige adipose cells with thermogenic activities [12, 29, 30]. Although cold stimulation was found to reduce lipid quantity in BAT [5] and WAT browning was associated with the creation of gap junctions [30], no study to date has assessed the effects of cold stimuli on collagen structures in the ECM of BAT. The present study therefore analyzed the cold-induced dynamic changes in the structure of collagen fibers in BAT. These results will enhance understanding of healthy adaptation to cold environments.

II.   Materials and Methods

Preparation of near infrared (NIR) fluorescent probes

The NIR fluorescent probes in the present study consisted of CNTs [10, 11] coated with phospholipid polyethylene glycol (PLPEG) and designated PLPEG-CNTs. These PLPEG-CNTs were prepared as previously described

[27]. Briefly, CNTs (HiPco, Lot No. R1-831, NanoIntegris, Inc., Skokie, IL, USA) were dispersed in an aqueous solution of sodium cholate (SC; 1% in weight; Sigma-Aldrich Co. LLC, St. Louis, MO, USA) using an ultrasonic homogenizer (Sonifier 250D, Branson Ultrasonics, Emerson Japan, Ltd. Kanagawa, Japan). The resulting suspension was centrifuged in an angle rotor (S50A, Hitachi Koki Co., Ltd. Tokyo, Japan). Approximately 70% of the resulting supernatant was collected. The CNTs were concentrated and the dispersant SC was exchanged for PLPEG using a centrifugal filter unit (Amicon Ultra-15 Ultracel-3, Merck Millipore Corp., Darmshtadt, Germany) by adding 2 mL of a 1% aqueous solution of PLPEG (i.e., 1,2-distearoyl-sn-glycero-3-phosphoethanolamine-N-[amino(poly(ethylene-glycol))-5000]; SUNBRIGHT® DSPE-050PA, NOF American Corporation, New York, NY, USA) to 10 mL of supernatant. The volume of the dispersion solution was halved by centrifugation through a centrifugal filter, with water added to restore the volume. This process was repeated 5–7 times to remove SC. The concentration of CNT was estimated from the optical absorbance of the solution at 280 nm, measured using a UV-vis-NIR spectrometer (UV-3600, Shimadzu, Kyoto, Japan). The final PLPEG-CNT dispersion solution was 2 mL in volume, with an estimated CNT concentration of 0.5 mg/mL. Its PLPEG concentration was estimated at 1% as the PLPEG did not pass through the centrifugal filter.

Mouse experiments

Female BALB/cAJcl-nu/nu nude mice, aged 7 weeks, were obtained from CLEA Japan Inc. (Tokyo, Japan) and allowed to acclimate to the institute laboratories for 1–3 weeks. Nude mice were used throughout this study, because hair could hamper the imaging of BAT and other organs, whereas the removal of hair could damage the, skin, resulting in the accumulation of the NIR fluorescent probe of PLPEG-CNTs at scratch sites. Three to five mice were housed in cages and allowed free access to food and water. They were housed individually during the cold exposure experiments.

Mice were exposed to cold temperature (10°C) for 19 hr. Where indicated, cold-exposed mice were returned to room temperature (25°C) for 19 hr. To assess the effects of cold stimulation on BAT or the systemic vasculature, some mice were injected in the tail vein with 0.1 mL PLPEG-CNT solution per mouse, equivalent to 2.5 mg CNT/kg/body weight, 5 hr before the end of cold stimulation. The mice were subsequently anesthetized by isoflurane inhalation (Pfizer Inc., New York, NY, USA) for whole-body imaging with the NIR camera.

Mice were euthanized by cardiac puncture under isoflurane anesthesia after cold stimulation or return to room temperature for 19 hr. Adipose tissues were collected, fixed with 10% formalin neutral buffer solution (Fujifilm Wako Pure Chemical Corporation) at room temperature for more than 1 week, and embedded in paraffin blocks.

For histological observation, tissue sections of thickness ~5 μm were sliced and mounted onto glass slides for tissue staining. The surfaces of the remaining blocks of embedded tissue were covered with paraffin for tissue preservation (paraffin (prev.)). These paraffin blocks were used to measure NIR fluorescent intensity of embedded tissues.

To measure the intensity of fluorescence emitted by a solid material, the surface must be flat and smooth to avoid random scattering of excitation light and emitted fluorescent light. The surfaces of the paraffin blocks (prev.) were made flat and smooth by slicing, allowing measurement of the NIR fluorescence intensity of CNTs accumulated in BAT.

All animal experiments were performed at the National Institute of Advanced Industrial Science and Technology (AIST) and Hokkaido University. Animal experiments performed at the AIST were approved by the Animal Care and Use Committee of AIST and were in accordance with the guidelines and regulations of the AIST manual of animal experiments. All animal procedures at Hokkaido University were in accordance with the guidelines of the Hokkaido University Manual for Implementing Animal Experimentation and the Association for Assessment and Accreditation of Laboratory Animal Care (AAALAC) International and were approved by the Animal Care and Use Committee of Hokkaido University (Approval number 19-0118).

Tissue staining

The silver impregnation method of tissue staining involved oxidation with $KMnO_4$, treatment with $FeNH_4(SO_4)_2$, and staining with ammonium-silver solution (Naoumenko-Feigin silver solution), consisting of $AgNO_3$ and NH_4OH [18]. In addition, tissue sections were stained with nuclear fast red, as the latter did not emit fluorescence over 1000 nm and therefore did not hinder the results of NIR fluorescence microscopy. Tissue samples were also stained with picrosirius red (Picro-Sirius Red Stain Kit; cyTek Laboratories, Logan, UT, USA), according to the manufacturer's protocol.

Near-infrared photoluminescence imaging

Near-infrared photoluminescence imaging was performed as described [26–28]. Mice were obliquely irradiated with a home-built imaging system containing a lamp (IP-307TCS, Lanics; 800-nm short pass filter, FIT Leadintex, Inc., Tokyo, Japan) emitting light with a wavelength of 730 nm. CNT-NIR fluorescence images were captured by an NIR camera (InGaAs-array video camera, NIRvana 640ST, Princeton Instruments, Trenton, NJ, USA) set above the mouse. An objective lens (Cosmicar, Pentax, RICOH Imaging Company, Ltd., Tokyo, Japan) and 1000 nm long-pass filter were used, and the NIR camera exposure time was 100 ms. In addition to its use in mouse imaging, this system was used to measure the NIR fluorescence intensity of BAT embedded in paraffin blocks.

Histological observation

Tissue samples were assessed histologically using an epi- and trans-illumination type optical microscope (BX-51 IR, Olympus Corp., Tokyo, Japan), with the epi-illumination used to assess NIR fluorescence and the trans-illumination used to assess bright field observations [27, 28]. NIR fluorescence was assessed using an Xe lamp (UXL-76XB, Ushio Inc., Tokyo Japan), a single-band bandpass filter (center, 708 nm; width, 75 nm; BrightLine®, Semrock, IDEX Corp, Lake Forest, IL, USA), a 785 nm laser single-edge laser-flat dichroic beam splitter (BrightLine®, Semrock, IDEX Corp.), an 808 nm best-value long-pass edge filter (EdgeBasicTM, Semrock, IDEX Corp), and a 1100 nm long-pass filter (Olympus, Tokyo, Japan). For bright filed observation, the light source was changed to a halogen lamp and the images were captured with a CCD camera (AUSB.3, 4203K, ARMS system Co., LTD., Tokyo, Japan) without the bandpass filter, the long-pass edge filter, and the long-pass filter.

III. Results

Effects of cold stimulation on iBAT structures

Female BALB/cAJl-nu/nu nude mice were kept in a cold environment (10°C) for 19 hr and sacrificed, and their adipose tissues were harvested. Cold stimuli reduced the weights of interscapular BAT (iBAT) (Fig. 1A: a), but did not significantly alter the weights of inguinal WAT (ingWATs) (Fig. 1A: b). Cold stimulation had no effect on body weights (Fig. 1A: c) or body temperatures (rectum) (Fig. 1A: d), ensuring that adaptive thermogenesis was not altered in these mice. Cold stimulation increased the specific gravity of iBATs, as evidenced by the sinking of both iBATs and axillary BATs (aBATs) from cold-stimulated mice in formalin solution. On the other hand, most of iBATs and aBATs from unstimulated mice floated (Fig. 1B). By contrast, WATs, including ingWATs, retroperitoneal WATs (rpWATs), and gonadal WATs (gWATs), floated in formalin solution with and without the cold stimuli. These results indicate that cold stimulation specifically influenced the character of BATs.

Cold stimuli also affected the histology of iBATs. Numerous lipid droplets were observed in the cytoplasm of BAs in unstimulated mice (Fig. 2a–b), and cell boundaries were clearly recognizable in iBATs (Fig. 2b, dotted line). In response to cold stimulation, however, the numbers and sizes of lipid droplets in BAs were significantly reduced and the nucleus-nucleus distances became closer (Fig. 2c). Surprisingly, cell boundaries became unrecognizable (Fig. 2c, blue ellipses), suggesting that cold stimuli induced certain crucial changes in the structure of the extracellular space of iBATs.

Because Col. III fibers are stained black by silver impregnation [24], histological changes in iBATs of cold-stimulated mice were analyzed in more detail by silver staining. In unstimulated mice, Col. III fibers surrounded
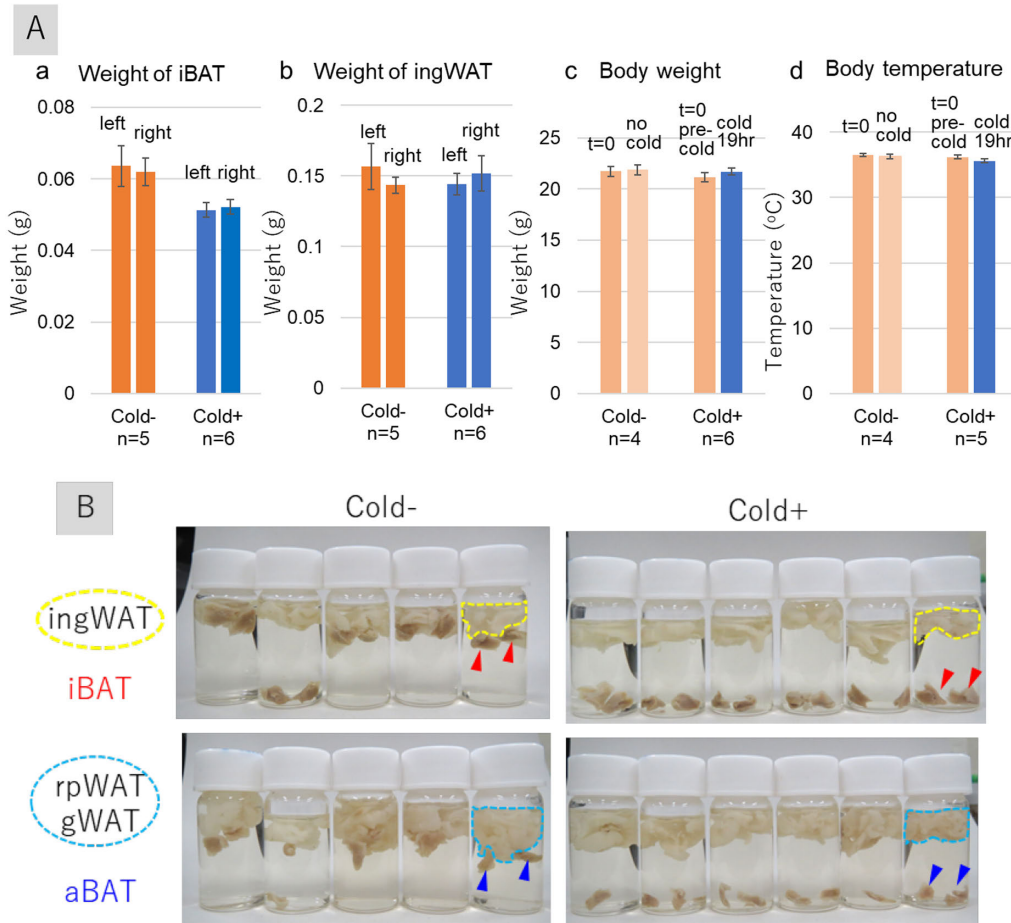
Fig. 1. Effects of cold stimulation on iBAT structures in female BALB/cAJcl-nu/nu mice. (**A**) Effects of cold stimulation (10°C, 19 hr) on the weights of iBAT (a) and ingWAT (b) and on body weight (c) and temperatures (d). Each bar represents the mean ± standard error of five or six mice exposed to cold stimulation (Cold+) and four or five control mice not exposed to cold stimulation (Cold−). (**B**) Photographs of formalin-fixed mouse tissue samples, showing iBAT, aBAT, ingWAT, rpWAT, and gWAT. Red and blue arrowheads indicate iBAT and aBAT, respectively. Areas surrounded by yellow dotted lines indicate ingWAT, and areas surrounded by sky-blue dotted lines indicate rpWAT and gWAT. Abbreviations: iBAT, interscapular brown adipose tissue; aBAT, axillary brown adipose tissue; ingWAT, inguinal white adipose tissue; rpWAT, retroperitoneal white adipose tissue; gWAT, gonadal white adipose tissue.
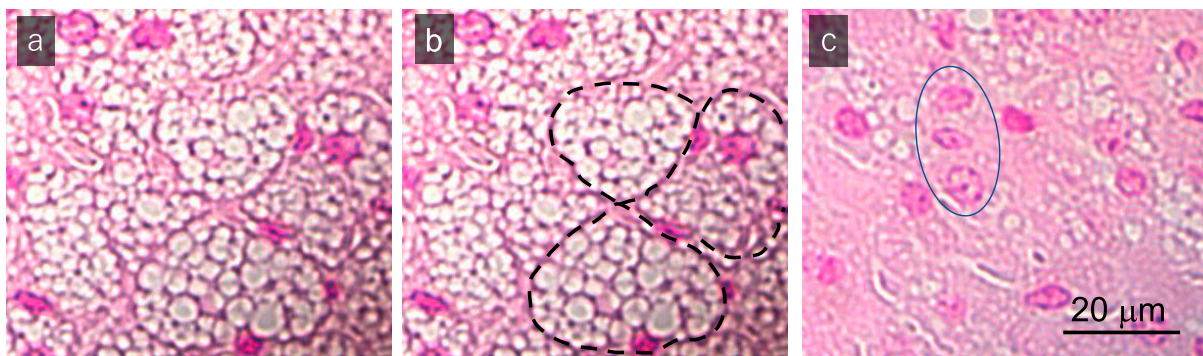

Fig. 2. Histological examination of nuclear fast red stained iBAT samples from (**a, b**) control mice not exposed to cold stimulation (Cold−) and (**c**) a mouse exposed to cold stimulation at 10°C for 4 hr (Cold+). The black dotted lines in (**b**) indicate cell boundaries. The blue ellipse in (**c**) denotes the site at which cell boundaries are hardly detectable. Results shown are representative of the findings in six mice each.
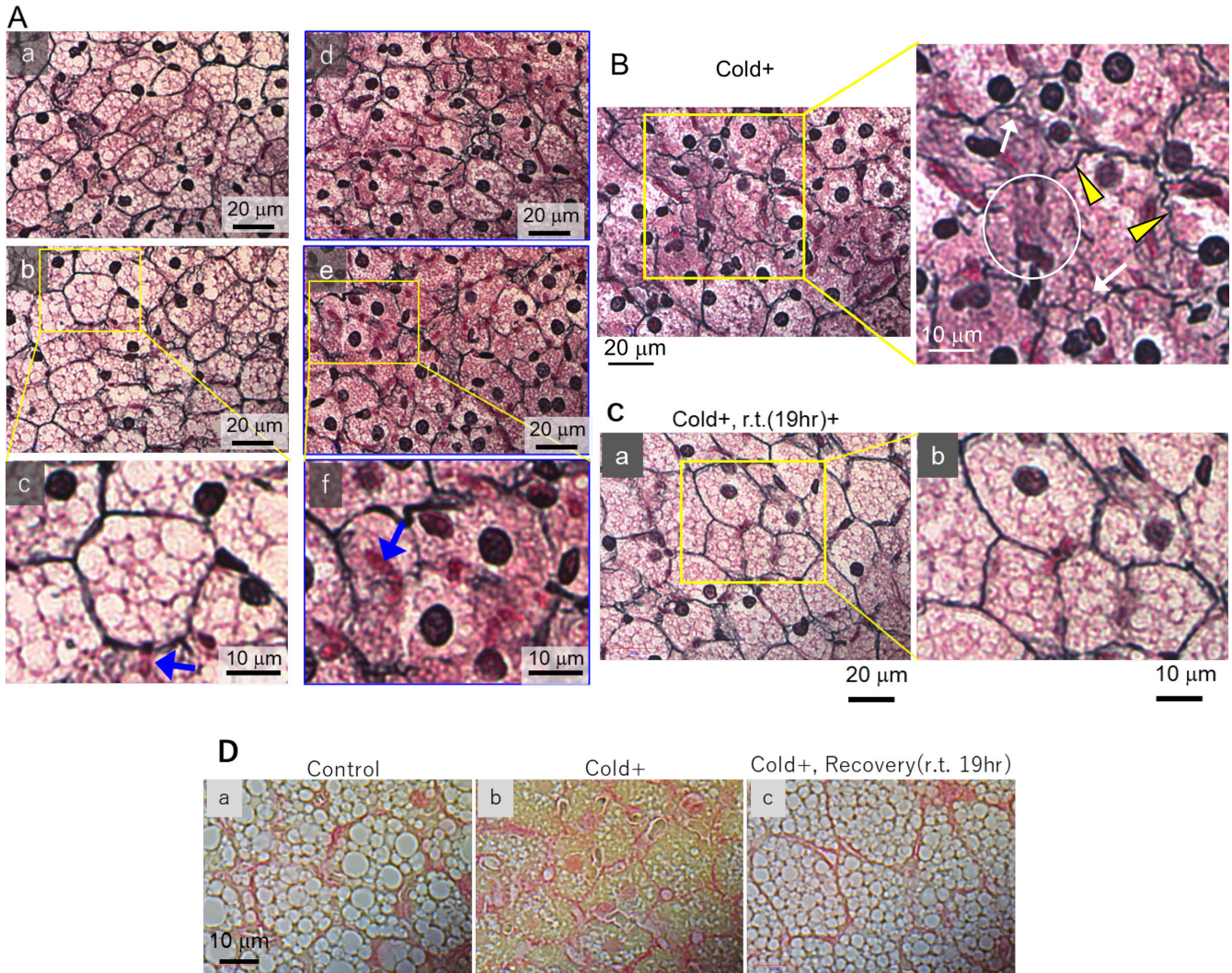
Fig. 3. Influence of cold stimuli on iBAT structure and its recovery. (**A–B**) Optical micrographs of silver-stained iBATs of mice not exposed (**A**: a–c) and exposed (**A**: d–f, **B**) to cold at 10°C for 19 hr. Results are representative of five mice each. Blue arrows indicate red blood cells (RBC); yellow arrowheads represent twisted fibers; white arrows indicate emancipated fibers; and white circles indicate curtailed areas. (**C**) Optical micrographs of silver-stained iBATs of mice exposed to cold at 10°C for 19 hr and subsequently kept at room temperature for 19 hr. Results are representative of four mice. (**D**) Micrographs of picosirius red-stained iBATs of mice (a) not exposed and (b) exposed to cold at 10°C for 19 hr and (c) of mice exposed to cold for 19 hr and subsequently kept to room temperature for 19 hr. Results are representative of four mice each.

the BAs, resulting in the formation of fine, well-arranged networks (Fig. 3A: a–c). Thin fibrils stained reddish purple were found on the surfaces of lipid droplets inside BAs (Fig. 3A: c). Each nucleus was stained dark (Fig. 3A: a–c), and red blood cells were stained red (Fig. 3A: c, blue arrow).

In response to cold stimulation, however, the well-organized networks of Col. III fibers in iBATs had broken down (Fig. 3A: d–f), in agreement with the structural changes previously observed in the extracellular space (Fig. 2C). At higher magnification, twisted (Fig. 3B, yellow arrowheads), emancipated (Fig. 3B, white arrows) and curtailed fibers (Fig. 3B, white circle) were frequently observed. Although reddish-purple fibrils were found to localize around lipid droplets in normal BAs (Fig. 3A: c),

the disappearance of lipid droplets following cold stimulation resulted in these fibrils become tangled and disseminating throughout the entire BA cytoplasm (Fig. 3A: f).

Despite the structures of Col. III fibers in iBAT being disordered in cold-stimulated mice, the structures promptly normalized, and the lipid-rich droplets reappeared, after the mice were maintained at room temperature for 19 hr (Fig. 3C). The reversibility of these alterations in iBAT structures suggests that the cold-induced disarrangement of the Col. III fibers and the other changes in iBAT are physiological reactions rather than pathological processes.

These findings were confirmed by Picrosirius Red staining, which can stain Col. III/Col. I fibers and cytosol red and yellow, respectively (Fig. 3D). Collagens stained red in the intercellular spaces in iBATs of unstimulated
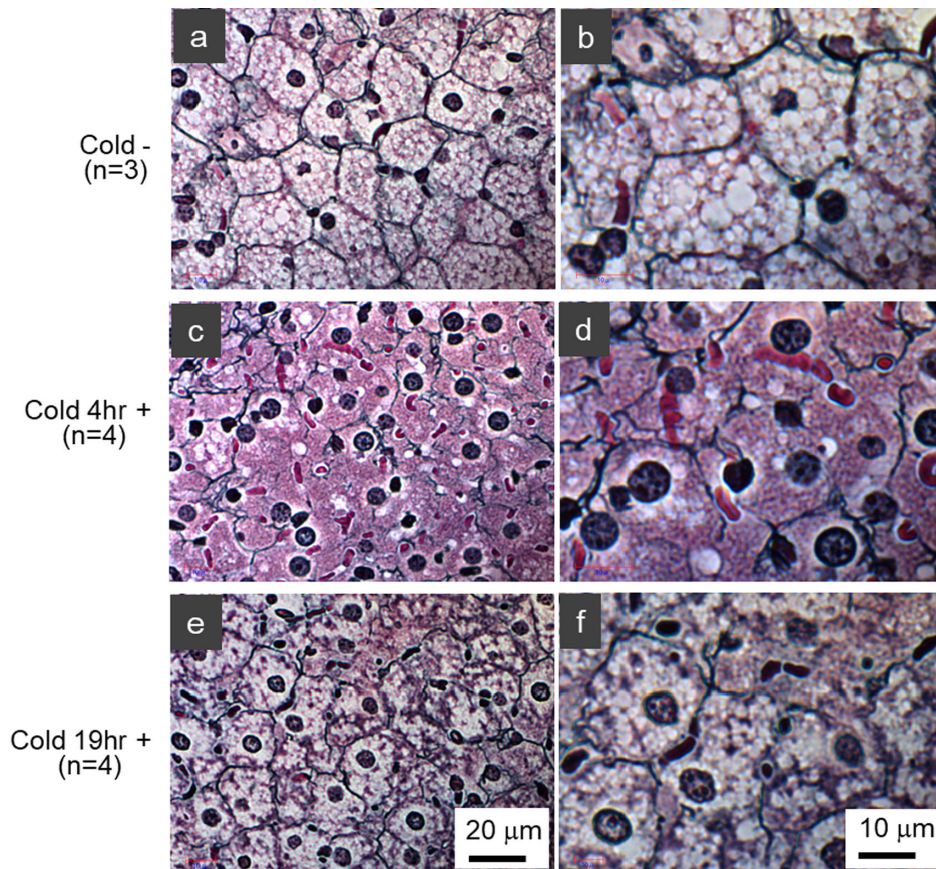
Fig. 4. Effect of duration of cold stimulation on the structural integrity of iBAT. Histological examination of silver-stained iBATs of (**a, b**) control mice and of mice exposed to cold at 10°C for (**c, d**) 4 hr and (**e, f**) 19 hr. The numbers of mice in each group (3 or 4) are indicated in the figure. The black color indicates type III collagen fibers.

mice (Fig. 3D: a) became disordered after cold stimulation (Fig. 3D: b) but recovered after these mice were maintained at room temperature for 19 hr (Fig. 3D: c).

Time course of structural changes in Col. III fibers

The degree of structural changes in iBAT Col. III fibers was found to depend on the duration of the cold stimulus: Normal structures were observed in the iBAT of control mice (Fig. 4a–b), whereas the structures of Col. III fibers exposed to the cold for 4 hr showed severely degenerated features (Fig. 4c–d). Interestingly, iBAT of mice exposed to the cold for 19 hr showed milder structural changes with the reappearance of lipid droplets (Fig. 4e–f), suggesting that a process of recovery may constitute an adaptation to a cold environment.

Enhanced vascular permeability of iBAT

We previously reported that fasting enhanced vascular permeability in iBAT of mice, as shown by the extravasation of the NIR fluorescent probe PLPEG-CNT [27]. CNTs [10, 11] are excellent NIR fluorescent agents [19], providing clear images of tissue due to the low absorbance and scattering of NIR light by the tissues as well as the low intensity of auto-fluorescence of the tissues at NIR wavelengths [8, 9, 22, 26–28]. We hypothesized that cold stimulation would enhance vascular permeability. To evaluate this hypothesis, PLPEG-CNTs were intravenously injected into the tail veins of cold-stimulated mice and their distribution was assessed 5 hr later by NIR fluorescence imaging (Fig. 5A). CNT-fluorescence was found to be brighter in iBATs of cold-stimulated than of unstimulated mice (Fig. 5B: a, b), with PLPEG-CNTs remaining in the vessels at 5 hr (Fig. 5B: c, d). To eliminate the influence of PLPEG-CNTs in vessels on the fluorescence intensity of iBATs, the mice were sacrificed by blood sampling and iBATs were harvested. CNT-fluorescence intensities of the harvested iBATs were measured after embedding them in paraffin blocks (cf. "Materials and Methods"). The fluorescence intensities of iBATs were higher in cold-stimulated than in unstimulated mice (Fig. 5C).

To determine intratissue distributions of PLPEG-CNTs in iBATs, tissue slices were assessed by NIR fluorescence microscopy. PLPEG-CNTs in iBATs of cold-stimulated mice were detected in the lumen of the arterioles (Fig. 6A: a–c, green arrow) and the capillaries (Fig. 6A: g, yellow arrows). PLPEG-CNTs were also detected in the intracellular regions (Fig. 6A: g, red arrowheads), especially in the perinuclear regions (Fig. 6A: g, yellow arrowheads). Their
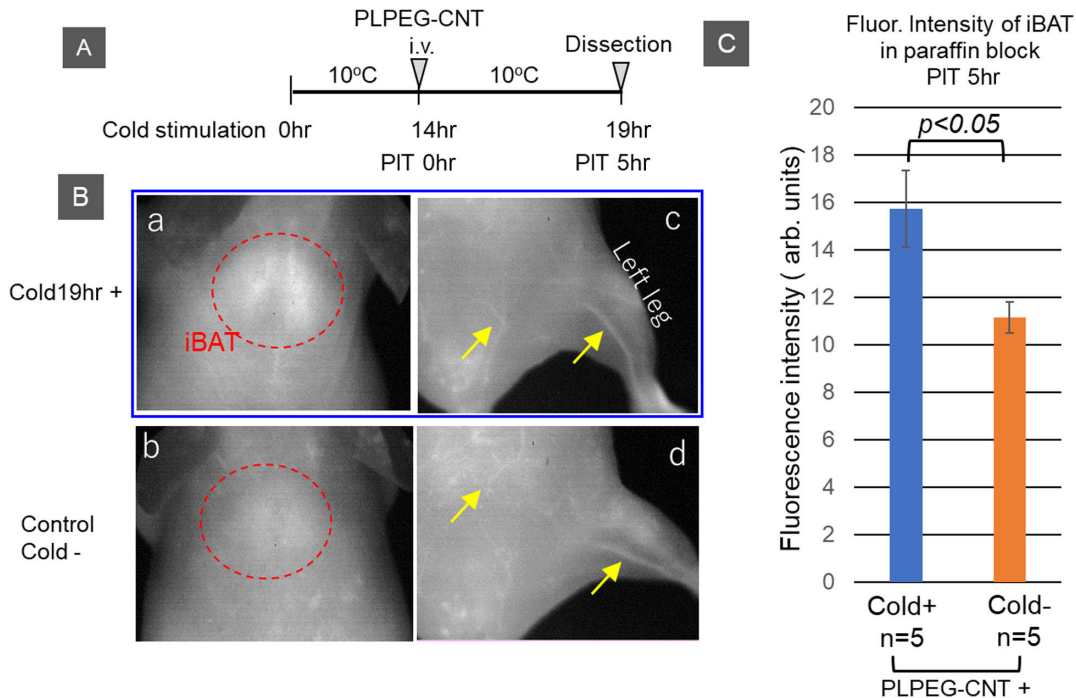
Fig. 5. Near infrared (NIR) fluorescent imaging of iBAT. (**A**) Timetable for cold stimulation, intravenous (iv) injection of NIR fluorescent imaging probe (PLPEG-CNT), and dissection. (**B**) Typical NIR fluorescence photos of the interscapular areas and abdomen/leg taken 5 hr after the iv injection of PLPEG-CNT into mice (a, c) exposed and (b, d) not exposed to cold stimulation at 10°C for 19 hr. Red circles indicate iBAT, and yellow arrows indicate veins. (**C**) NIR fluorescence intensities after subtraction of background fluorescence of iBATs obtained 5 hr after the iv injection of PLPEG-CNT into mice (blue) exposed and (orange) not exposed to cold stimulation at 10°C for 19 hr (see the text for the details of the method). Error bars denote mean ± standard errors. CNT NIR fluorescence intensities differed between the Cold+ group and Cold− group according to T-test analysis.

presence in both extracellular and intracellular regions indicates that PLPEG-CNTs were extravasated from the vessels, distributed in intercellular spaces and even taken up by BAs. By contrast, the magnitude of extravasation of PLPEG-CNTs was significantly lower in the iBATs of unstimulated than of stimulated mice, although similar levels of PLPEG-CNTs was observed in the arterioles (Fig. 6B: a–f) and capillaries (Fig. 6B: g). These results indicate that the extravasation of PLPEG-CNTs is a cold-stimulation-dependent phenomenon.

Structural changes of ingWATs

In agreement with findings showing that cold stimulation did not alter the weight or specific gravity of ingWATs, histologic examination of ingWATs showed no significant changes in response to either cold stimulation or recovery (Fig. S1 in Supplementary Materials). In contrast, cold stimulation enhanced the vascular permeability of ingWATs as well as iBATs, as evidenced by the accumulation of PLPEG-CNT NIR fluorescence in phagocytic cells located in lymph nodes within ingWATs (Figs. S2 and S3 in Supplementary Materials).

IV. Discussion

BATs are a unique tissue, showing prompt changes in size and structure in response to life crises, especially in situations requiring a boost in thermogenesis. Cold stimulation is one these crises, in which stored triglycerides are consumed for thermogenesis, causing shrinkage of lipid droplets and reductions in the total volume of BAs and the weight of BAT. In addition, the structure of Col. III fibers in ECM drastically changes, as shown in the current study.

Collagens in the ECM of iBAT and their remodeling

Analysis of WAT has shown that Col. IV is the major collagen in the basal lamina of ECM surrounding white adipocytes [20] and that Col. VI is specific to adipocytes [16]. Col. VI is a stiff collagen, generated more in *ob/ob* than in normal mice. This is advantageous for obese *ob/ob* mice, enabling the tight retention of large-sized white adipocytes. The sizes of lipid droplets and white adipocytes are larger in Col.VI knockout than in wild-type *ob/ob* mice, partly due to the reduced mechanical restriction of Col. VI fibers [13].

Less is known, however, about the collagens in ECM of BATs. Treatment with glucocorticoids, which activates ECM remodeling, has been reported to increase the amount of collagen in BAT, although the details have not been described [17]. Although the ratio of Col. IV to Col. VI was shown to be important for the differentiation of adipocytes, details regarding the regulation of their expression, as well as the regulation of other types of collagen, remain elusive [4].
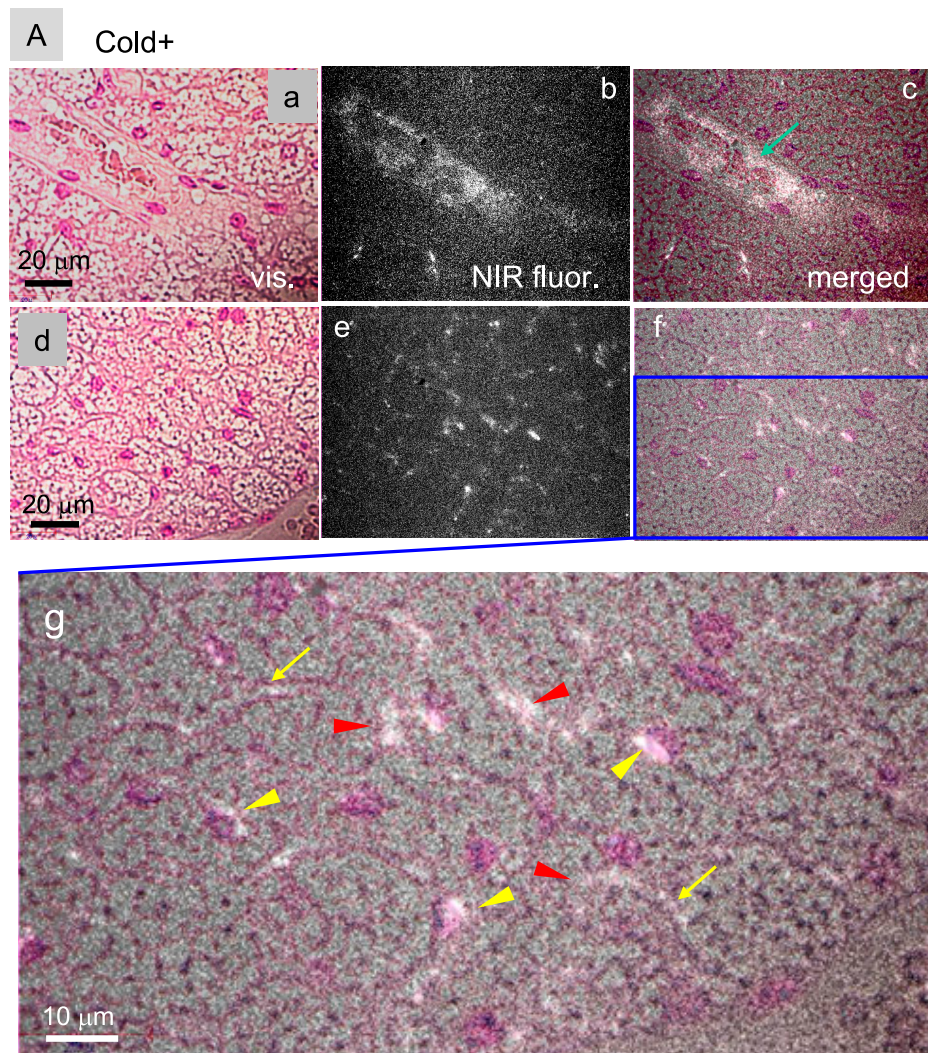
Fig. 6. Near infrared (NIR) fluorescence micrographs of nuclear fast red-stained iBATs of (**A**) cold-stimulated and (**B**) unstimulated mice. iBATs were harvested 5 hr after the iv injection of PLPEG-CNT. In both panels, (a) and (d) represent visible-light transmission micrographs, (b) and (e) represent NIR fluorescent micrographs, and (c) and (f) represent merged images of (a) and (b) and of (d) and (e), respectively, with (g) representing the magnified image of the blue rectangular area in (f). White spots, CNT fluorescence; green arrow, PLPEG-CNTs in arterioles; yellow arrow, PLPEG-CNT in capillaries; red arrowheads, PLPEG-CNTs in intercellular spaces; yellow arrowheads, PLPEG-CNTs in perinuclear regions. Each micrograph is representative of five mice per group.

The current study showed that Col. III fibers are abundant in iBAT, as confirmed by Ag impregnation staining [22, 24]. The presence of Col. III fibers in iBAT seems reasonable because Col. III fibers can hold cells and lobular structures of soft tissues and organs, including the liver, spleen, and lymph nodes, without causing strong mechanical stress.

Exposure of mice to cold environments results in the curtailment, emancipation, and twisting of Col. III fibers in iBAT, with these structural disarrangements returning to normal within a short period of time when mice are kept at room temperature. These findings indicate that Col. III is significantly involved in regulating ECM structures by rearrangement of higher-order structures. This hypothesis is in good agreement with general concepts about the functions of Col. III. For example, Col. III was found to colocalize with Col. I, controlling the fibrogenesis of the latter and the morphogenesis of cardiovascular systems, as evidenced by Ehlers–Danlos syndrome (aortic rupture), which is caused by Col. III gene mutations [15]. Alternatively, Col. III can serve as a covalent modifier of the Col. II fiber network in cartilage, inasmuch as Col. III polymeric filaments are interwoven with and cross-linked to Col. II fibrillar networks [25].

The present study showed that Col. III fibers are an important constituent of the collagen architecture in ECM of BATs. Although details about other components of collagens in ECM of BATs remain elusive, future studies may increase understanding of ECM remodeling of BAT in response to environmental changes.
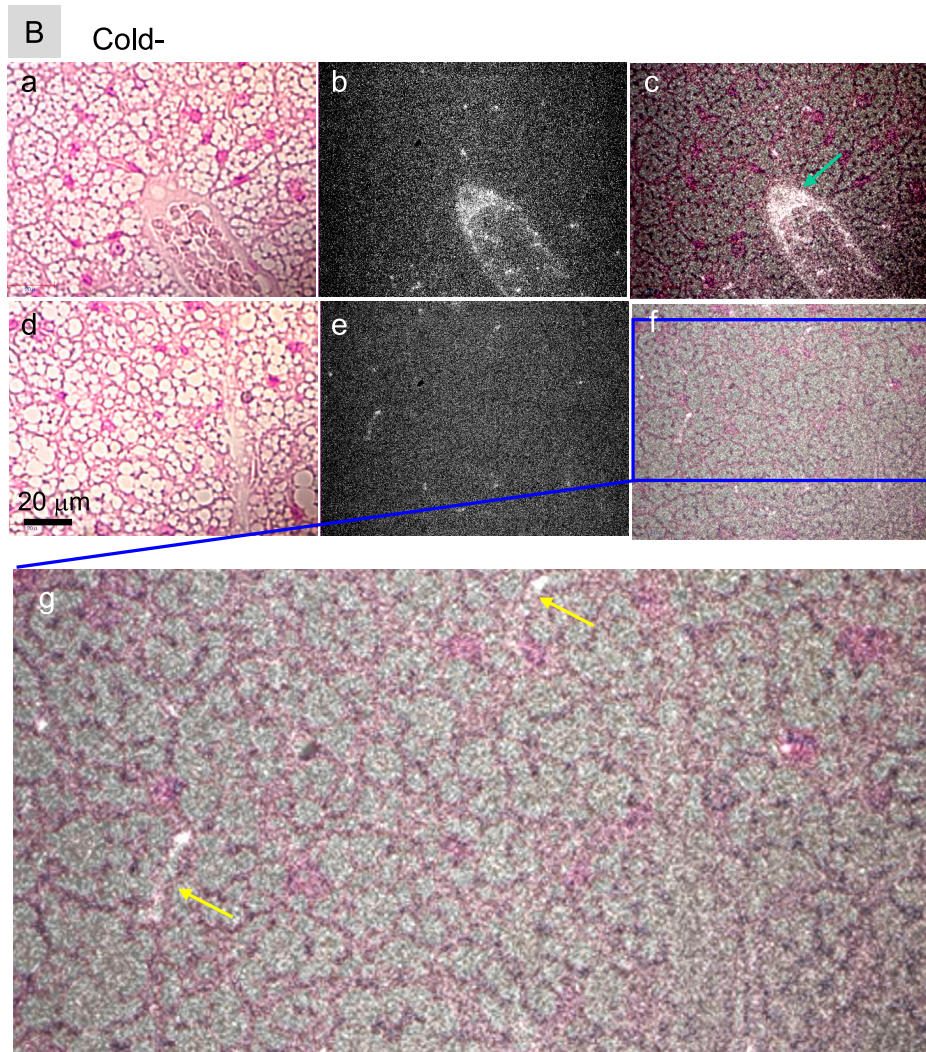
Fig. 6. Continued.

Ag-staining-positive subcellular fibrous structures in BAs

In addition to being present in extracellular spaces, this study found that Ag-staining-positive fibrous structures were present in intracellular regions of BAs, especially around lipid droplets.

Vimentin fibrils are known as intermediate filaments, the arrangement of which is altered from an extended fibrillar to a complex cage formation tightly associated with the formation of lipid globules [7]. Therefore, the fibrils detected around lipid droplets in BA of unstimulated mice and those distributed within the cytoplasm of BA of cold stimulated mice might be composed of vimentin fibrils. Although vimentin is ubiquitously expressed as a component of intermediate filaments, differences among other components would impart specific characteristics to each fibrous structure in individual cells. Destruction/reconstitution systems operate in both intra- and extra-cellular fibrous networks when the sizes of lipid droplets in BA dynamically change in response to environmental shifts, such as fasting/refeeding [27] and cold/rewarming. Additional studies, however, are required to determine the precise molecular mechanisms.

NIR fluorescence imaging and microscopy

Biological systems are highly transparent to NIR wavelengths > 1000 nm, making NIR light useful for imaging inside the body. Few materials emit NIR fluorescence, making CNTs one of the few candidates for effectual live imaging probes. The use of CNTs as NIR fluorescence probes enabled the clear imaging of mouse vasculature, even deep within the body [8, 9, 15, 21]. In addition to their usefulness in whole-body imaging, CNTs are useful in histological examinations. The distribution of CNTs in tissues and cells can be evaluated by NIR fluorescent microscopy, without disturbance by tissue autofluorescence. A drawback of NIR fluorescence imaging is its penetration depth in the body. Because CNT NIR fluorescence cannot be evaluated at a depth greater than a couple of centimeters,

NIR fluorescent microscopy has not yet become common for live imaging of large sized mammals. In addition, the number of NIR fluorescent materials currently available is limited, with an increase in this number required for the further development of NIR fluorescent imaging and microscopy.

In conclusion, this study showed that exposure of mice to a cold environment resulted in a shrinkage of iBAT, resulting from the consumption of stored lipids in BA for thermogenesis. Moreover, Col. III fibers in ECM of iBATs became twisted, emancipated, and curtailed, and vascular permeability was enhanced. Intracellularly, Ag-stained-positive fibrous structures in BAs, possibly vimentin fibrils, became disordered. These unusual changes, however, were promptly reversed when the mice were kept at room temperature for 19 hr, indicating that the changes were physiological reactions to adapt to cold environments. Because similar changes in iBAT were observed in fasting mice [27], the dynamic structural changes of ECM provide BATs with high flexibility in the regulation of their sizes and vascular permeability in response to environmental changes.

V.   Conflicts of Interest

The authors declare no potential conflicts of interest that may be related to the content of the manuscript, including funding, employment, or personal financial interests.

VI.   Acknowledgments

VII.   References

1. Azhdarinia, A., Daquinag, A. C., Tseng, C., Ghosh, S. C., Ghosh, P., Amaya-Manzanares, F., *et al.* (2013) A peptide probe for targeted brown adipose tissue imaging. *Nat. Commun.* 4; 2472.

2. Bartelt, A., Bruns, O. T., Reimer, R., Hohenberg, H., Ittrich, H., Peldschus, K., *et al.* (2011) Brown adipose tissue activity controls triglyceride clearance. *Nat. Med.* 17; 200–205.

3. Beck, K. Types of collagen fibers. https://sciencing.com/types-collagen-fibers-6880209.html (Last access date: March 31, 2021)

4. Carobbio, S., Guénantin, A.-C., Samuelson, I., Bahri, M. and Vidal-Puig, A. (2019) Brown and beige fat: From molecules to physiology and pathophysiology. *Biochim. Biophys. Acta Mol. Cell Biol. Lipids* 1864; 37–50.

5. Coolbaugh, C. L., Damon, B. M., Bush, E. C., Welch, E. B. and Towse, T. F. (2019) Cold exposure induces dynamic, heterogeneous alterations in human brown adipose tissue lipid content. *Sci. Rep.* 9; 13600.

6. Dong, M., Yang, X, Lim, S., Cao, Z., Honek, J., Lu, H., *et al.* (2013) Cold exposure promotes atherosclerotic plaque growth

and instability via UCP1-dependent lipolysis. *Cell Metab.* 18; 118–129.

7. Franke, W. W., Hergt, M. and Grund, C. (1987) Rearrangement of the vimentin cytoskeleton during adipose conversion: formation of an intermediate filament cage around lipid globules. *Cell* 49; 131–141.

8. Hong, G., Diao, S., Chang, J., Antaris, A. L., Chen, C., Zhang, B., *et al.* (2014) Through-skull fluorescence imaging of the brain in a new near-infrared window. *Nat. Photonics* 8; 723–730.

9. Hong, G., Lee, J. C., Robinson, J. T., Raaz, U., Xie, L., Huang, N. F., *et al.* (2012) Multifunctional in vivo vascular imaging using near-infrared II fluorescence. *Nat. Med.* 18; 1841–1846.

10. Iijima, S. (1991) Helical microtubules of graphitic carbon. *Nature* 354; 56–58.

11. Iijima, S. and Ichihashi, T. (1993) Single-shell carbon nanotubes of 1-nm diameter. *Nature* 363; 603–605.

12. Jang, C., Jalapu, S., Thuzar, M., Law, P. W., Jeavons, S., Barclay, J. L., *et al.* (2014) Infrared thermography in the detection of brown adipose tissue in humans. *Physiol. Rep.* 2; e12167.

13. Khan, T., Muise, E. S., Iyengar, P., Wang, Z. V., Chandalia, M., Abate, N., *et al.* (2009) Metabolic dysregulation and adipose tissue fibrosis: role of collagen VI. *Mol. Cell. Biol.* 29; 1575–1591.

14. Lee, Y.-H., Petkova, A. P., Konkar, A. A. and Granneman, J. G. (2015) Cellular origins of cold-induced brown adipocytes in adult mice. *FASEB J.* 29; 286–299.

15. Liu, X., Wu, H., Byrne, M., Krane, S. and Jaenisch, R. (1997) Type III collagen is crucial for collagen I fibrillogenesis and for normal cardiovascular development. *Proc. Natl. Acad. Sci. U S A* 94; 1852–1856.

16. Mariman, E. C. and Wang, P. (2010) Adipocyte extracellular matrix composition, dynamics and role in obesity. *Cell. Mol. Life Sci.* 67; 1277–1292.

17. Mousovich-Neto, F., Matos, M. S., Costa, A. C. R., de Melo Reis, R. A., Atella, G. C., Miranda-Alves, L., *et al.* (2019) Brown adipose tissue remodelling induced by corticosterone in male Wistar rats. *Exp. Physiol.* 104; 524–528.

18. Naoumenko, J. and Feigin, I. (1963) A modification for paraffin sections of silver carbonate impregnation for microglia. *Acta Neuropathol.* 3; 402–406.

19. O'Connell, M. J., Bachilo, S. M., Huffman, C. B., Moore, V. C., Strano, M. S., Haroz, E. H., *et al.* (2002) Band gap fluorescence from individual single-walled carbon nanotubes. *Science* 297; 593–596.

20. Pierleoni, C., Verdenelli, F., Castellucci, M. and Cinti, S. (1998) Fibronectins and basal lamina molecules expression in human subcutaneous white adipose tissue. *Eur. J. Histochem.* 42; 183–188.

21. Robinson, J. T., Welsher, K., Tabakman, S. M., Sherlock, S. P., Wang, H., Luong, R., *et al.* (2010) High performance in vivo near-IR (> 1 μm) imaging and photothermal cancer therapy with carbon nanotubes. *Nano Res.* 3; 779–793.

22. Shiga University of Medical Science, Lecture of histology, 8th, Connective Tissue and ECM. http://www.shiga-med.ac.jp/~hqanat2/pdf/2017histolgy.8.pdf (in Japanese).

23. Soga, K., Umezawa, M. and Okubo, K. (Eds.) (2021) Transparency in Biology. Making the Invisible Visible, Springer, Singapore.

24. Ushiki, T. (2002) Collagen fibers, reticular fibers and elastic fibers. A comprehensive understanding from a morphological viewpoint. *Arch. Histol. Cytol.* 65; 109–126.

25. Wu, J.-J., Weis, M. A., Kim, L. S. and Eyre, D. R. (2010) Type III collagen, a fibril network modifier in articular cartilage. *J. Biol. Chem.* 285; 18537–18544.

26. Yomogida, Y., Tanaka, T., Zhang, M., Yudasaka, M., Wei, X.

and Kataura, H. (2016) Industrial-scale separation of high-purity single-chirality single-wall carbon nanotubes for biological imaging. *Nat. Commun.* 7; 12056.

27. Yudasaka, M., Yomogida, Y., Zhang, M., Nakahara, M., Kobayashi, N., Tanaka, T., *et al.* (2018) Fasting-dependent vascular permeability enhancement in brown adipose tissues evidenced by using carbon nanotubes as fluorescent probes. *Sci. Rep.* 8; 14446.

28. Yudasaka, M., Yomogida, Y., Zhang, M., Tanaka, T., Nakahara, M., Kobayashi, N., *et al.* (2017) Near-infrared photoluminescent carbon nanotubes for imaging of brown fat. *Sci. Rep.* 7; 44760.

29. Zhang, X., Tian, Y., Zhang, H., Kavishwar, A., Lynes, M.,

Brownell, A. L., *et al.* (2015) Curcumin analogues as selective fluorescence imaging probes for brown adipose tissue and monitoring browning. *Sci. Rep.* 5; 13116.

30. Zhu, Y., Gao, Y., Tao, C., Shao, M., Zhao, S., Huang, W., *et al.* (2016) Connexin 43 mediates white adipose tissue beiging by facilitating the propagation of sympathetic neuronal signals. *Cell Metab.* 24; 420–433.